Effects of minijets on azimuthal harmonics in relativistic heavy-ion collisions at RHIC and LHC

Jinbiao Hu[1], Lilin Zhu[1], Hua Zheng[2*], Rudolph C. Hwa[3]
[1] *Department of Physics, Sichuan University, Chengdu 610064, China;*
[2] *School of Physics and Information Technology, Shaanxi Normal University, Xi'an 710119, China;*
[3] *Institute of Fundamental Science, University of Oregon, Eugene, Oregon 97403-5203, USA.*

The production of hadrons in heavy-ion collisions at the low transverse momentum (p_T) is investigated in the framework of recombination model (RM) with emphasis on the effects of minijets on azimuthal anisotropy. The azimuthal anisotropy of produced hadrons is generated by the minijets both through energy loss to the hot dense medium and in creating shower partons that recombine with the thermal partons. Harmonic analysis of the ϕ dependence leads to $v_2(p_T, b)$ for pions and protons that agree with data for a wide range of colliding energies from $\sqrt{s_{NN}} = 7.7$ GeV to 5.02 TeV. At the same time, the p_T and centrality dependencies of the higher harmonic coefficients v_3 and v_4 for pions and protons are prescribed by the interplay between (thermal)-thermal-thermal and (thermal)-thermal-shower recombination components. It is shown that v_3 and v_4 for pions and protons at $\sqrt{s_{NN}} = 200$ GeV, 2.76 and 5.02 TeV can be well reproduced. Additionally, predictions of the higher harmonic coefficients v_3 and v_4 for pions and protons at the BNL Relativistic Heavy Collider (RHIC) Beam Energy Scan (BES) energies are presented.

PACS numbers:

I. INTRODUCTION

Collisions of heavy nuclei have been exploited for decades to search for and study the transition from the hadronic matter to quark gluon plasma (QGP) at the BNL Relativistic Heavy Ion Collider (RHIC) and the CERN Larger Hadron Collider (LHC) [1–3]. In these collisions, the expanded overlap area does not possess spherical symmetry. In non-central collisions, the overlap area is roughly elliptic in shape. This spatial anisotropy of the overlap region is transformed into the anisotropy in momentum space initially through interactions between partons and at later stages between the produced particles. The azimuthal anisotropy of identified particles is one of the most striking observations when studying the characteristics of the QGP.

In hydrodynamical studies, azimuthal anisotropy of produced hadrons in non-central collisions is ascribed to the consequence of asymmetric pressure gradient in the transverse plane at early time, assuming fast thermalization [4–7]. Such an early time of equilibration has never been shown to be the consequence of any dynamical process that is firmly grounded and commonly accepted. However, it is not the only approach that can claim physical relevance.

An alternative view is to regard semihard scattering near the surface of the nuclear overlap as the driving force of the azimuthal anisotropy, since at low enough virtuality such scattering processes are pervasive throughout the medium. When they occur near the surface of the initial configuration of the hot dense system, the semihard partons can emerge from the medium and not only hadronize as intermediate-p_T jets, but also generate ridge particles at lower p_T [8–10]. Actually, a theoretical description of the connection between ridges and the second harmonic coefficient v_2 in the approximation of using a simple geometrical picture was presented [9, 10]. The ridge particles were assumed to have the same azimuthal angle ϕ distribution as that of the enhanced thermal partons. In Ref. [11], we investigated the hadron production at low p_T produced in Au+Au collisions at $\sqrt{s_{NN}} = 200$ GeV within the recombination model (RM) including the effects of minijets on the azimuthal anisotropy. It was shown that the azimuthal anisotropy of the ridges produces the observed second harmonic v_2 at low p_T [10, 11]. For higher harmonic coefficients, such as v_3 and v_4, it is widely accepted that they are due to the fluctuations of the initial configuration [12, 13]. In RM, minijets affect the low p_T region through thermal-shower (TS) or thermal-thermal-shower (TTS) recombination, which plays a similar role of the fluctuations of the initial configuration. It was shown that, within the framework of RM, the centrality dependence of higher harmonic coefficients v_3 and v_4 for pions produced in Au+Au collisions at $\sqrt{s_{NN}} = 200$ GeV were well reproduced [11]. In this study, we will extend the investigation of the azimuthal anisotropy for a wide range of colliding energies from $\sqrt{s_{NN}} = 7.7$ GeV to 5.02 TeV in Au+Au and Pb+Pb collisions at RHIC and LHC with emphasis on the effects of minijets and conclude with a summary on our general view of the azimuthal anisotropy in relativistic nuclear collisions.

The paper is organized as follows. In Sec. II, we briefly review the basic framework of the recombination model, including the inclusive distribution of minijets. The formalisms of the azimuthal harmonics are shown in Sec. III. In Sec. IV, we show results from our study on the centrality dependence of the azimuthal harmonic coef-

*Corresponding author: zhengh@snnu.edu.cn

ficients $v_n(p_T, b)$ $(n = 2, 3, 4)$ for pions and protons in Au+Au collisions at $\sqrt{s_{NN}} = 7.7 - 200$ GeV and Pb + Pb collisions at $\sqrt{s_{NN}} = 2.76$ and 5.02 TeV. Finally, Sec. V summarizes the results and gives the conclusion.

II. COMMON FORM OF HADRONIC SPECTRA

We begin with a recapitulation of the formalism for single-particle distribution from the recombination model [14–16]. The invariant distributions of pions and protons production at midrapidity are expressed as

$$p^0\frac{dN^\pi}{dp_T} = \int\left(\prod_{i=1}^{2}\frac{dq_i}{q_i}\right)F_{q\bar{q}}(q_1,q_2)\mathcal{R}_\pi(q_1,q_2,p_T), \quad (1)$$

$$p^0\frac{dN^p}{dp_T} = \int\left(\prod_{i=1}^{3}\frac{dq_i}{q_i}\right)F_{qqq}(q_1,q_2,q_3)\mathcal{R}_p(q_1,q_2,q_3,p_T). \quad (2)$$

$\mathcal{R}_h$ $(h = \pi, p)$ is the recombination function (RF). For pions and protons, we have [14–16]

$$\mathcal{R}_\pi(q_1,q_2,p_T) = \frac{q_1q_2}{p_T^2}\delta\left(\sum_{i=1}^{2}\frac{q_i}{p_T}-1\right), \quad (3)$$

$$\mathcal{R}_p(q_1,q_2,q_3,p_T) = g_{st}^p g_p(\frac{q_1q_2}{p_T^2})^\alpha(\frac{q_3}{p_T})^\beta\delta\left(\sum_{i=1}^{3}\frac{q_i}{p_T}-1\right), \quad (4)$$

where $g_{st} = 1/6$, $\alpha = 1.75$, $\beta = 1.05$ and

$$g_p = [B(\alpha+1,\alpha+\beta+2)B(\alpha+1,\beta+1)]. \quad (5)$$

$B(a, b)$ is the Beta function. In RM, the partons are divided into two types: thermal (T) and shower (S). The former contains the medium effect, and the latter is due to the semihard and hard scattered partons. Therefore, the parton distributions are partitioned into several components,

$$F_{q\bar{q}} = \mathcal{TT}+\mathcal{TS}+\mathcal{SS}, \quad (6)$$

$$F_{qqq} = \mathcal{TTT}+\mathcal{TTS}+\mathcal{TSS}+\mathcal{SSS}, \quad (7)$$

where $\mathcal{T}$ and $\mathcal{S}$ are the invariant distributions of thermal and shower partons, respectively. At low p_T, only thermal parton recombination needs to be considered. The thermal partons are assumed to behave as

$$\mathcal{T}(q_i) = q_i\frac{dN_q}{dq_i} = Cq_ie^{-q_i/T}. \quad (8)$$

The parameter T is treated as an inverse slope. It possesses a scaling law that is universal across all hadrons, which has been studied in our previous works [17, 18]. The values are listed in Table I. Then the hadron distribution at low p_T can be written as

$$\frac{dN_h^{\mathrm{TT(T)}}}{p_Tdp_T} = \mathcal{N}_h(p_T,c)e^{-p_T/T}. \quad (9)$$

$\sqrt{s}$	5020	2760	200	62.4	39	27	19.6	14.5	11.5	7.7
T	0.42	0.39	0.3	0.263	0.25	0.243	0.233	0.226	0.222	0.217

Table I: Values of T in GeV/c for listed $\sqrt{s_{NN}}$ in GeV.

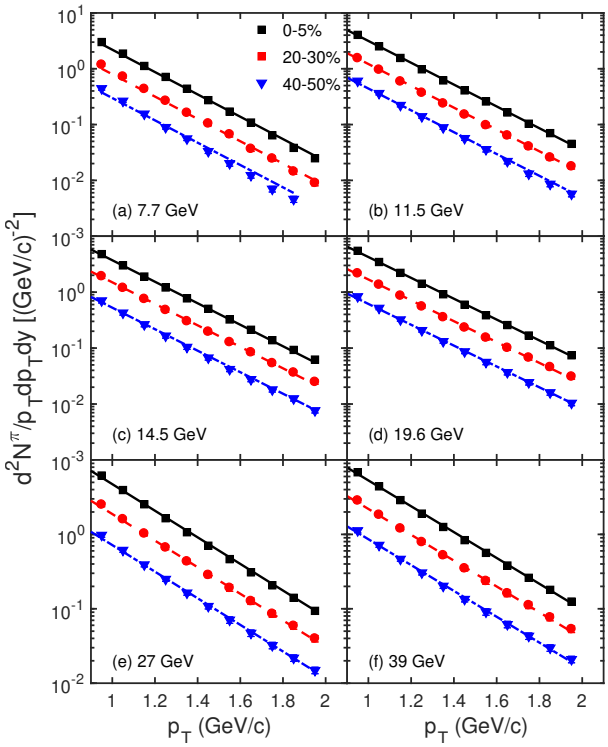

Figure 1: Transverse momentum spectra of pions for the centralities of 0-5%, 20-30% and 40-50% in Au+Au collisions at $\sqrt{s_{NN}} = 7.7$, 11.5, 14.5, 19.6, 27 and 39 GeV. The lines are the fits with Eq. (9). The data are from Ref. [19].

The normalization factor $\mathcal{N}^h(p_T, c)$ depends on centrality c. It is then clear that the proton distribution having C^3 dependence and the pions distribution being $\propto C^2$. As shown in the earlier work [18], the transverse momentum spectra of protons for various centralities can be well described by Eq. (9) in Au+Au collisions at $\sqrt{s_{NN}} = 7.7$, 11.5, 19.6, 27 and 39 GeV. Having determined T, we have no more freedom to adjust the exponential behavior of the pion spectra. The transverse momentum spectra for pions in Au+Au collisions at $\sqrt{s_{NN}} = 7.7$, 11.5, 14.5, 19.6, 27 and 39 GeV and 0-5%, 20-30% and 40-50% centralities are shown in Fig. 1. Obviously, the experimental p_T distribution of pions at low p_T establishes the exponential behavior. Furthermore, with our earlier work for Au+Au collisions at $\sqrt{s_{NN}} = 62.4$ and 200 GeV as well as Pb+Pb collisions at 2.76 and 5.02 TeV [17, 18], the excellent agreement supports the assertion that both pion and proton spectra at low p_T can be described by the same T in the exponential factor for a wide range of collision energies

from $\sqrt{s_{NN}} = 7.7$ GeV to 5.02 TeV. It should be pointed out that the basic formulas for recombination shown in Eqs. (1) and (2) are valid for the direct production of all hadrons from thermal partons. For proton production TTT recombination is prevalent at $p_T < 2$ GeV/c. For pions from resonance decays that are important for $p_T < 1$ GeV/c, Eq. (1) is inadequate to describe them. Furthermore, when the contributions from shower partons is not negligible even at $p_T < 2$ GeV/c, appropriate equations will be given and discussed in the next section.

III. AZIMUTHAL ANISOTROPY

We now broaden our consideration to include the azimuthal angle ϕ dependence by considering the effects of semihard partons. For non-central collisions the initial almond-shaped configuration leads to ϕ anisotropy. As done in Ref. [11], $\rho^h(p_T, \phi, b)$ denotes the single-particle distribution of hadron h produced at mid-rapidity in heavy-ion collisions at impact parameter b

$$\rho^h(p_T, \phi, b) = \frac{dN_h}{p_T dp_T d\phi}(p_T, \phi, b). \tag{10}$$

At low p_T, ρ^h is assumed to consist of three components

$$\rho^h(p_T, \phi, b) = B^h(p_T, b) + R^h(p_T, \phi, b) + M^h(p_T, \phi, b), \tag{11}$$

referring as Base, Ridge and Minijet components, respectively. The base component that has no preferred direction to expand is isotopic and becomes the background of the ridge and minijet components that carry all the information about the anisotropy of the initial geometry. In recombination model, the first two components are due to the recombination of thermal partons, while the third is dependent of thermal-shower (TS) for pions or thermal-thermal-shower recombination (TTS) for protons [14], which is dominant in the intermediate p_T region ($2 < p_T < 6$ GeV/c), but is still not negligible at low p_T [20]. After averaging over ϕ, we have

$$\bar{\rho}^h(p_T, b) = B^h(p_T, b) + \bar{R}^h(p_T, b) + \bar{M}^h(p_T, b). \tag{12}$$

Semihard partons, created near the surface and directed outward, can give rise to ϕ anisotropy in the thermal component. That is because each such semihard parton loses some energy to the medium, thereby enhancing the thermal motion of the soft partons near its trajectory. Those thermal partons eventually lead to hadrons at late time that are dependent on the azimuthal angle of the semihard parton. In Refs. [9, 20] those hadrons are identified with ridge that stands above the background with characteristic peaking in ϕ. Ridge is a phenomenon characterized by an extended range in pseudorapidity η and a narrow range in ϕ [21]. It was found that the azimuthal correlation between a semihard parton and a ridge hadron formed by TT recombination for pions can be described by a Gaussian distribution in ϕ with a width $\sigma = 0.33$ in order to reproduce the ridge data [22]. The more detailed discussion for the ϕ dependence of thermal partons will be given in the next section.

Shower partons can arise from semihard and hard partons created throughout the medium in random directions. Because of jet quenching the partons that emerge from the medium have reduced momenta, and the distribution of the shower partons generated by subsequent fragmentation peaks at low p_T. They recombine with the thermal partons and therefore form hadrons that have approximately the same ϕ angles as the initiating semihard or hard partons. After averaging over all events, the azimuthal dependence of the TS or TTS component can have all harmonic components, which are described by the third term $M^h(p_T, \phi, b)$ in Eq. (11). The formulas of TS and TTS components for pions and protons at a specified centrality c are shown as follows, respectively [15, 16],

$$\frac{dN_\pi^{TS}}{p_T dp_T} = \frac{C}{p_T^3}\int_0^{p_T} dp_1 p_1 e^{-p_1/T}\left[\mathcal{S}^u(p_T - p_1, c) + \mathcal{S}^{\bar{d}}(p_T - p_1, c)\right], \tag{13}$$

$$\frac{dN_p^{TTS}}{p_T dp_T} = \frac{g_{st}^p g_p C^2}{m_T^p p_T^{2\alpha+\beta+3}}\int_0^{p_T} dp_1 \int_0^{p_T - p_1} dp_2\, e^{-(p_1+p_2)/T}\left\{(p_1 p_2)^{\alpha+1}(p_T - p_1 - p_2)^\beta \mathcal{S}^d(p_T - p_1 - p_2, c) + p_1^{\alpha+1} p_2^{\beta+1}(p_T - p_1 - p_2)^\alpha \mathcal{S}^u(p_T - p_1 - p_2, c)\right\}, \tag{14}$$

with the shower parton distribution after integration over jet momentum k is

$$\mathcal{S}^j(p_2, c) = \xi_{\rm eff}\,\sigma_g \int_{k_0}^\infty dk k f_g(k, c) S_g^j(p_2/k). \tag{15}$$

$\sqrt{s_{NN}}$ [GeV]	A [1/GeV^2]	B [GeV]	n
7.7	171	2.7311	11.570
11.5	256	2.6068	11.205
14.5	322	2.535	10.994
19.6	436	2.4416	10.271
27	601	2.3423	10.429
39	868	2.2284	10.095
62.4	1389	2.0827	9.668

Table II: Parameters for $f_g(k)$ for Au+Au collisions at $\sqrt{s_{NN}} = 7.7 - 62.4$ GeV.

The factor $\sigma_g = 1.2$ is taken to consider the other (semi)hard partons whose contributions are approximated by adding 20% to that from gluon jets [23]. The parameter $\xi_{\rm eff} = 0.07$ is the average suppression factor that is related to the nuclear modification factor R_{AA} [14]. $f_g(k, c)$ is the initial transverse momentum distribution of gluons at midrapidity. For central collisions, a simple parameterization is given as follows [24]

$$f_g(k, 0.05) = K\frac{A}{(1 + k/B)^n}, \tag{16}$$

where $c = 0.05$ stands for 0-10% centrality. For Pb+Pb collisions at 2.76 and 5.02 TeV, the parameters A, B and n were obtained by logarithmic interpolations of $\ln A$, B and n between Au+Au collisions at 200 GeV and Pb+Pb collisions at 5.5 TeV [16]. For the lower BES energies, we adopt the logarithmic extrapolation to calculate the parameters for f_g, which are listed in Table II with $K = 2.5$. S_g^j is the unintegrated shower parton distribution (SPD) in a jet of gluon fragmentation into a parton of type j with momentum fraction p_2/k. It is determined from the fragmentation function (FF) considering that hadrons in a jet are formed by recombination of the shower partons in the jet [14]. Including the centrality dependence, the initial gluon jet distribution is assumed as [15, 16]

$$f_g(k, c) = \frac{T_{AA(c)}}{T_{AA}(0.05)} f_g(k, 0.05), \tag{17}$$

with the nuclear thickness function T_{AA}.

IV. HARMONIC COEFFICIENTS

The detailed calculations for the second harmonic coefficient of ϕ anisotropy $v_2(p_T, b)$ and the higher harmonic coefficients v_n with $n = 3, 4$ were presented in Ref. [11]. We only briefly review the approach for the present study. With Eq. (11), the harmonic coefficients can be expressed as

$$v_n^h(p_T, b) = \langle \cos n\phi \rangle_\rho^h = \frac{\int_0^{2\pi} d\phi \cos n\phi \rho^h(p_T, \phi, b)}{\int_0^{2\pi} d\phi \rho^h(p_T, \phi, b)}. \tag{18}$$

The second component of $\rho^h(p_T, \phi, b)$, $R(p_T, \phi, b)$, contains the ϕ dependence due to the initial elliptical spatial configuration through the $S(\phi, b)$ function, which is the segment of the surface through which the semihard parton is emitted to contribute to a ridge particle with the azimuthal angle ϕ. It transforms the spatial to momentum asymmetry. The derivation of $S(\phi, b)$ given in Ref. [20] is based on the geometry of the initial configuration taken to be an ellipse with width w and height h, where $w = 1 - b/2$ and $h = (1 - b^2/4)^{1/2}$ in units of nuclear radius R_A,

$$S(\phi, b) = h(b)[E(\theta_2, \alpha) - E(\theta_1, \alpha)], \tag{19}$$

where $E(\theta_i, \alpha)$ is the elliptic integral of the second kind with $\alpha = 1 - w^2/h^2$ and

$$\theta_i = \tan^{-1}\left(\frac{h}{w}\tan\phi_i\right), \quad \phi_1 = \phi - \sigma, \quad \phi_2 = \phi + \sigma, \tag{20}$$

for $\phi_i \leq \pi/2$, and an analytic continuation of it for $\phi_2 > \pi/2$. It should be noted that $S(\phi, b)$ in Eq. (19) is not normalized. Since the elliptical axes may not coincide with the reaction plane that contains the impact parameter b, a tilt angle ψ_2 is introduced and averaged over,

$$\tilde{S}_2(\phi, b) = \frac{2}{\pi}\int_{\pi/4}^{\pi/4} d\psi_2 S_2(\phi - \psi_2, b). \tag{21}$$

So the normalized $\tilde{S}_2(\phi, b)$ can be expressed as,

$$S_2(\phi, b) = \tilde{S}_2(\phi, b) \Big/ \frac{1}{2\pi}\int_0^{2\pi} d\phi \tilde{S}_2(\phi, b)\ . \tag{22}$$

Then, the ridge component of ρ^h that responds to the minijets through TT or TTT recombination can be written as

$$R^h(p_T, \phi, b) = S(\phi, b)\bar{R}^h(p_T, b), \tag{23}$$

while the ϕ-independent base thermal component is expressed as

$$B^h(p_T, b) = \mathcal{N}_h(p_T, b)e^{-p_T/T_0}, \tag{24}$$

where T_0 is treated as a free parameter, which is the colliding energy dependence and the values will be shown in the next section. With Eq. (8), the enhanced ridge component is

$$\bar{R}^h(p_T, b) = \mathcal{N}_h(p_T, b)[e^{-p_T/T} - e^{-p_T/T_0}]. \tag{25}$$

When considering the higher harmonics, the minijets affect the low-p_T region through TS or TTS recombination. Since minijets are produced in unpredictable directions, the average ϕ distribution can have all terms in a harmonic analysis. As done for $R^h(p_T, \phi, b)$ in Eq. (23), we write the third component of $\rho^h(p_T, \phi, b)$ as

$$M^h(p_T, \phi, b) = J(\phi, b)\bar{M}^h(p_T, b), \tag{26}$$

where $J(\phi,b)$ describes the ϕ-dependent part of the minijet contribution, which is assumed as

$$J(\phi,b)=\tilde{J}(\phi,b)\Big/\frac{1}{2\pi}\int_0^{2\pi}d\phi\tilde{J}(\phi,b)\ , \tag{27}$$

where $\tilde{J}(\phi,b)$ contains all the harmonic components, $\cos n\phi$, averaged over the tilt anlge ψ_n,

$$\tilde{J}(\phi,b)=1+b\sum_{n=2}^{\infty}a_n\frac{n}{\pi}\int_{-\pi/2n}^{\pi/2n}d\psi_n\cos n(\phi-\psi_n), \tag{28}$$

where $a_n, n\geq 2$, are free parameters to be determined by fitting the experimental data of v_n.

With the three components of $\rho^h(p_T,\phi,b)$ shown in Eqs. (23), (24) and (26), a universal formula for the azimuthal harmonics from Eq. (18) can be obtained

$$v_n^h(p_T,b)=\frac{\langle\cos n\phi\rangle_S\,\bar{R}^h(p_T,b)+\langle\cos n\phi\rangle_J\,\bar{M}^h(p_T,b)}{\bar{\rho}^h(p_T,b)}, \tag{29}$$

where

$$\langle\cos 2\phi\rangle_S = \frac{1}{2\pi}\int_0^{2\pi}d\phi\cos 2\phi S(\phi,b), \tag{30}$$

$$\langle\cos n\phi\rangle_J = \frac{1}{2\pi}\int_0^{2\pi}d\phi\cos n\phi J(\phi,b). \tag{31}$$

$\langle\cos n\phi\rangle_S$ in Eq. (30) is equal to zero for $n\geq 3$ because of the periodicity of $S(\phi,b)$. Whereas $\langle\cos n\phi\rangle_J$ receives contribution only from the a_n term in Eq. (28) because of the orthogonality of the harmonics.

V. RESULTS AND DISCUSSION

So far, we have discussed the azimuthal anisotropy with the effects from semihard scattering near the surface of the nuclear overlap. The azimuthal harmonic coefficients $v_n(p_T,b)$ $(n=2,3,4)$ for pions in Au+Au collisions at $\sqrt{s_{NN}}=200$ GeV was studied in our earlier work [11]. In this work, the investigation is extended to Au+Au collisions at $\sqrt{s_{NN}}=7.7$, 11.5, 14.5, 19.6, 27, 39 and 62.4 GeV as well as Pb+Pb collisions at both $\sqrt{s_{NN}}=2.76$ and 5.02 TeV with the same framework.

Figure 2 shows the second harmonic coefficient $v_2(p_T,b)$ of pions (black solid lines) and protons (red dashed lines) in Au+Au collisions at $\sqrt{s_{NN}}=7.7$, 11.5, 14.5, 19.6, 27, 39, 62.4 and 200 GeV from the recombination model. Also shown in the figure are the elliptic flow of pions (solid circles) and protons (red triangles) from RHIC Collaboration [25, 26] for Au+Au collisions at centralities of 0-10%, 10-40% and 40-80%, respectively. Compared with our earlier work for $\sqrt{s_{NN}}=200$ GeV [11], the result for pions is recalculated due to the update of the parameter T in Ref. [18]. It must be emphasized that for protons, the mass effect should be taken into account. Specifically, p_T in Eqs. (24) and (25) should be replaced by the transverse kinetic energy $E_T(p_T)=m_T(p_T)-m_p$. Evidently, the agreement with the data is excellent for each centrality at every colliding energy where data exist in Fig. 2. Therefore, it is worth evaluating for the higher colliding energies $\sqrt{s_{NN}}=2.76$ and 5.02 TeV. Figure 3 shows the second harmonic coefficient v_2 of pions and protons in Pb+Pb collisions at $\sqrt{s_{NN}}=2.76$ and 5.02 TeV for the centralities of 0-5%, 10-20%, 20-30% and 30-40%. It is remarkable that the theoretical curves agree with the experimental data in Figs. 2 and 3 by only adjusting two parameters T_0 and a_2 for each colliding energy. The parameters T_0 and a_2 for the nine colliding energies are listed in TABLE III.

$\sqrt{s_{NN}}$ [GeV]	T_0 [GeV]	a_2	a_3	a_4
7.7	0.212	0.40	2.63	1.76
11.5	0.218	0.48	2.52	1.68
14.5	0.222	0.48	2.45	1.64
19.6	0.227	0.50	2.37	1.58
27	0.235	0.58	2.28	1.51
39	0.243	0.60	2.18	1.44
62.4	0.256	0.64	2.05	1.35
200	0.245	0.60	1.66	1.13
2760	0.385	0.78	1.18	0.74
5020	0.413	0.82	0.71	0.40

Table III: The values of parameters for T_0, a_2, a_3 and a_4 for Au+Au collisions at $\sqrt{s_{NN}}=7.7$, 11.5, 14.5, 19.6, 27, 39, 62.4, 200 GeV as well as Pb+Pb collisions at $\sqrt{s_{NN}}=2.76$ and 5.02 TeV.

For higher harmonic coefficients v_3 and v_4, the contribution from the third component $M^h(p_T,\phi,b)$ generated by TS or TTS recombination become important. It should be emphasized that T_0 has already been determined by fitting the second harmonic coefficient a_2, so it it not adjustable to fit the third and fourth harmonic coefficients v_3 and v_4. Using Eqs. (29) and (31) with $n=3$, $v_3(p_T,b)$ for pions and protons for various centralities at each colliding energy are calculated by adjusting a_3. Shown in the three panels to the bottom of Fig. 4 are the results at 0-10%, 10-40% and 40-80% for $\sqrt{s_{NN}}=200$ GeV, respectively. Results from our calculations give a nice description of the measured $v_3(p_T,b)$ of protons up to 2 GeV at these centralities. On the other hand, the third harmonic coefficient v_3 of pions for non-central collisions from the recombination model, shown by the black solid lines, are smaller than the experimental data from the STAR Collaboration [26]. For the higher colliding energies $\sqrt{s_{NN}}=2.76$ and 5.02 TeV, as shown by the lines in Fig. 5, the experimental $v_3(p_T,b)$ for both pions and protons can be well reproduced with the only one parameter a_3 for each colliding energy. Similarly, the

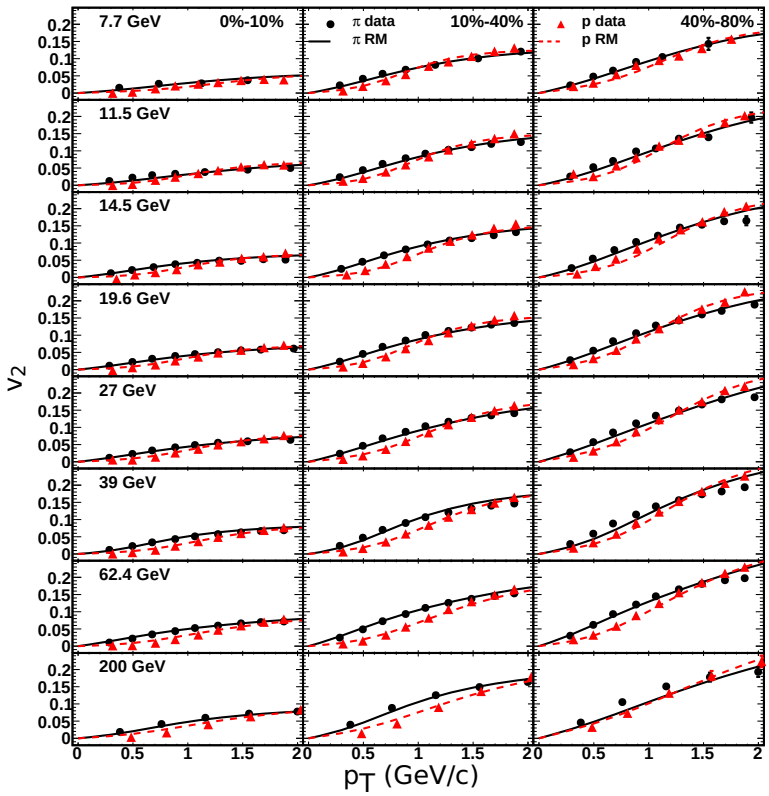

Figure 2: The second harmonic coefficient v_2 of pions and protons as a function of transverse momentum for the centralities of 0-10%, 10-40% and 40-80% in Au+Au collisions at $\sqrt{s_{NN}} = 7.7$, 11.5, 14.5, 19.6, 27, 39, 62.4 and 200 GeV. The lines are fits with Eq. (29). The data are from Refs. [25, 26].

fourth azimuthal harmonic coefficient $v_4(p_T, b)$ for pions and protons can be evaluated. For $\sqrt{s_{NN}} = 200$ GeV shown in Fig. 6, the fits for pions and protons are excellent for various centralities. The results for higher energies $\sqrt{s_{NN}} = 2.76$ and 5.02 TeV are presented in Fig.7. For pions, the theoretical calculations are smaller than the experimental data at small p_T but larger at larger p_T at both energies, while it is seen that the recombination model gives an overall quantitative description of $v_4(p_T, b)$ of protons in Pb+Pb collisions at $\sqrt{s_{NN}} = 2.76$ and 5.02 TeV. The corresponding values of a_3 and a_4 for $\sqrt{s_{NN}} = 200$ GeV, 2.76 and 5.02 TeV are shown in TABLE III. Unfortunately, the experimental data for the higher harmonic coefficients v_3 and v_4 at lower BES energies are not available yet. To make the prediction of higher harmonics for the lower BES energies, a linear relationship between the parameters a_n $(n = 3, 4)$ and $\ln\sqrt{s_{NN}}$ is parametrized. With the values of a_3 and a_4 for $\sqrt{s_{NN}} = 200$ GeV, 2.76 and 5.02 TeV listed in TABLE III, we can obtain,

$$a_3 = -0.274 \ln(\sqrt{s_{NN}}) + 3.187, \tag{32}$$

$$a_4 = -0.198 \ln(\sqrt{s_{NN}}) + 2.166, \tag{33}$$

where $\sqrt{s_{NN}}$ is in units of GeV. With Eqs. (32) and (33), the values of a_3 and a_4 for the lower BES energies are calculated and given in TABLE III. Therefore, we can predict the third and fourth harmonic coefficients of pions and protons in Au+Au collisions at $\sqrt{s_{NN}} = 7.7$, 11.5, 14.5, 19.6, 27, 39 and 62.4 GeV, which are shown in Figs. 4 and 6, respectively. These results can be checked by the experimental flow analysis results in the future.

VI. CONCLUSION

To summarize, we have shown that the major properties of pion and proton production at low p_T can be reproduced in our formulation of hadronization that includes the effects of minijets for a wide range of colliding enengies from $\sqrt{s_{NN}} = 7.7$ GeV to 5.02 TeV. The spectra for pions and protons at low p_T validate exponential behavior, $\exp(-p_T/T)$, with a common value of T that is the same as that of the thermal partons just before hadronization. Minijets generate azimuthal anisotropy both through energy loss to the medium and in creating shower partons that recombine with the thermal partons. Harmonic analysis of the ϕ-dependence leads to $v_n(p_T, b)$ $(n = 2, 3, 4)$ that agrees with the experimental data, even for the collisions at LHC where the density of semihard partons is so high initially that the system has insufficient time for equilibration before the abundant minijets

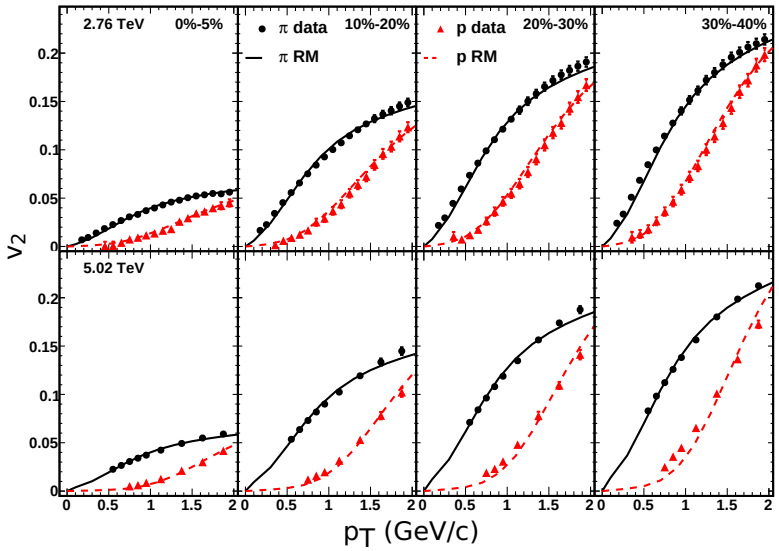

Figure 3: Same as Fig. 2 but for Pb+Pb collisions at $\sqrt{s_{NN}} = 2.76$ and 5.02 TeV at the centralities of 0-5%, 10-20%, 20-30% and 30-40%. The data are from Refs. [27, 28].

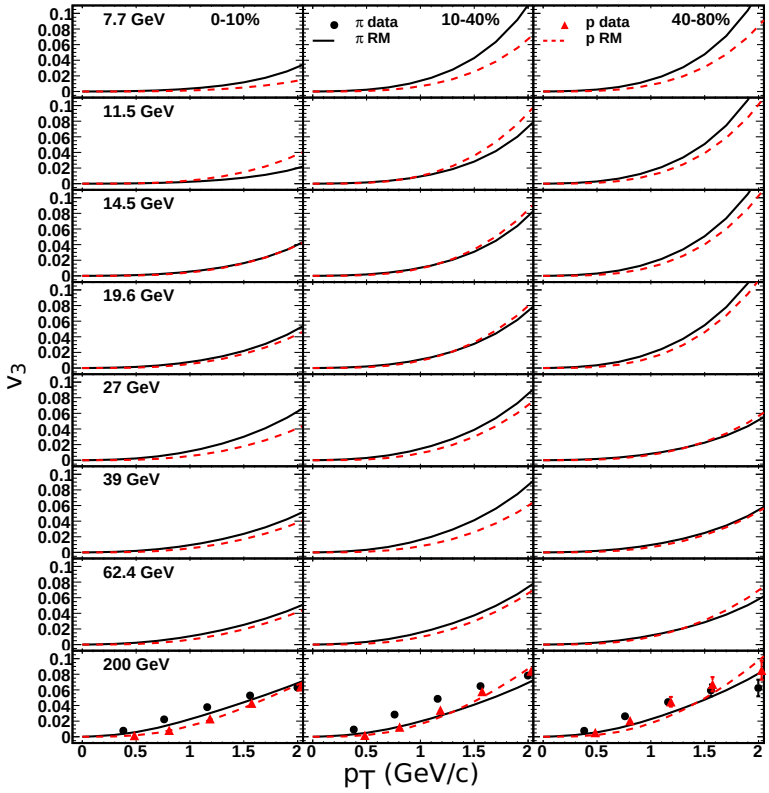

Figure 4: v_3 of pions and protons as a function of p_T in Au+Au collisions at $\sqrt{s_{NN}} = 7.7 - 200$ GeV for 0-10%, 10-40% and 40-80% centrality intervals. The lines are fits with Eq. (29). The data for $\sqrt{s_{NN}} = 200$ GeV are from Ref. [26].

created near the surface dominate the expansion characteristics.

This study is mainly a demonstration that minijets are important for the hadron production and azimuthal anisotropy, and can explain all the low-p_T data in the recombination framework. Furthermore, semihard partons created near the surface of the nuclear overlap can lead to a continuous range of ridges that is shaped by the initial geometry. We have also predicted the higher harmonic coefficients v_3 and v_4 for pions and protons in Au+Au

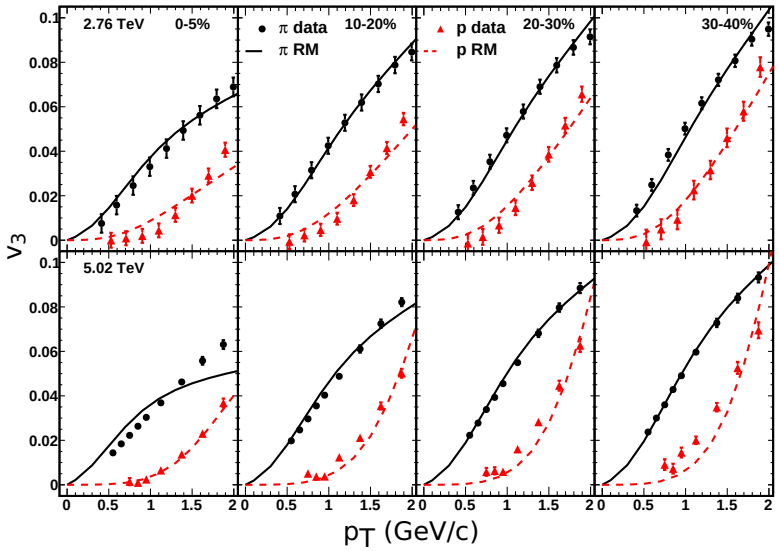

Figure 5: Same as Fig. 4 but for Pb+Pb collisions at $\sqrt{s_{NN}} = 2.76$ and 5.02 TeV at the centralities of 0-5%, 10-20%, 20-30% and 30-40%. The data are from Refs. [27, 28].

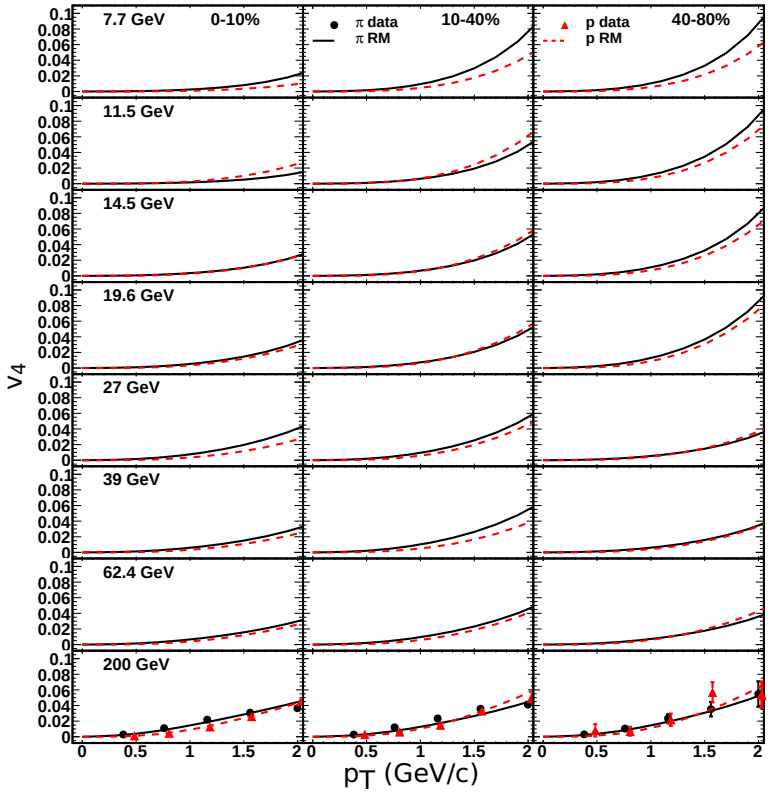

Figure 6: v_4 of pions and protons as a function of p_T in Au+Au collisions at $\sqrt{s_{NN}} = 7.7 - 200$ GeV for 0-10%, 10-40% and 40-80% centrality intervals. The lines are fits with Eq. (29). The data for $\sqrt{s_{NN}} = 200$ GeV are from Ref. [26].

collisions at lower BES energies, which can be compared with the experimental measurements in the future.

Acknowledgment

This work was supported in part by the National Natural Science Foundation of China under Grants No.

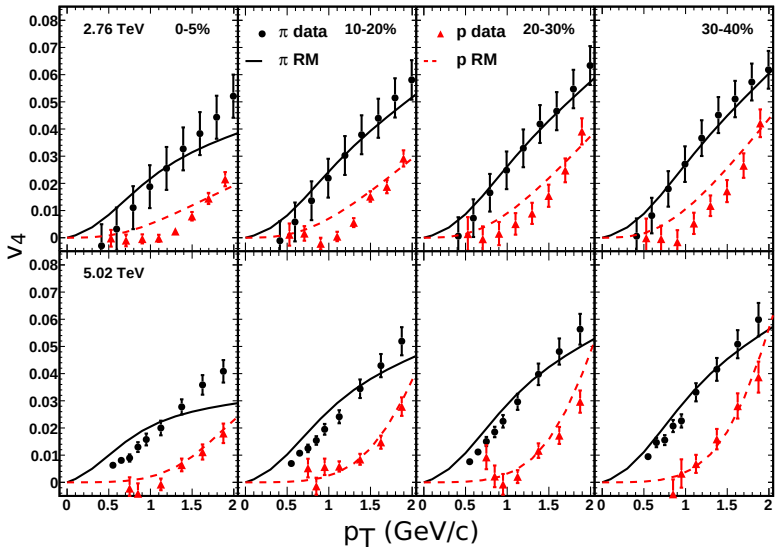

Figure 7: Same as Fig. 6 but for Pb+Pb collisions at $\sqrt{s_{NN}} = 2.76$ and 5.02 TeV at the centralities of 0-5%, 10-20%, 20-30% and 30-40%. The data are from Refs. [27, 28].

11905120 and No. 11947416, by the Natural Science Foundation of Sichuan Province under Grant No. 2023NSFSC1322.

[1] X. Luo and N. Xu, Nucl. Sci. Tech. **28**, 112 (2017).
[2] N. Armesto, in *Quark-Gluon Plasma 4*, ed. by R. C. Hwa and X. N. Wang (World Scientific, Singapore, 2010).
[3] N. Herrmann, J. P. Wessels and T. Wienold, Ann. Rev. Nucl. Part. Sci. **49**, 581-632 (1999).
[4] P. F. Kolb and U. Heinz, in *Quark-Gluon Plasma 3* ed. by R. C. Hwa and X. N. Wang (World Scientific, Singapore, 2004).
[5] U. Heinz and R. Snellings, Ann. Rev. Nucl. Part. Sci. **63**, 123-151, (2013).
[6] H. Song, S. A. Bass and U. Heinz, Phys. Rev. C **83**, 024912 (2011).
[7] W. Zhao, C. M. Ko, Y. X. Liu, G. Y. Qin and H. Song, Nucl. Phys. A **1005**, 121876 (2021).
[8] C. B. Chiu and R. C. Hwa, Phys. Rev. C **72**, 034903(2005).
[9] R. C. Hwa, Phys. Lett. B **666**, 228 (2008).
[10] C. B. Chiu, R. C. Hwa and C. B. Yang, Phys. Rev. C **78**, 044903 (2008).
[11] R. C. Hwa and L. Zhu, Phys. Rev. C **86**, 024901 (2012).
[12] B. Schenke, S. Jeon and C. Gale, Phys. Rev. C **85**, 024901 (2012).
[13] F. G. Gardim, F. Grassi, M. Luzum and J. Y. Ollitrault, Phys. Rev. Lett. **109**, 202302 (2012).
[14] R. C. Hwa and C. B. Yang, Phys. Rev. C **70**, 024905 (2004).
[15] L. Zhu and R. C. Hwa, Phys. Rev. C **88**, 044919 (2013).
[16] L. Zhu, H. Zheng and R. C. Hwa, Phys. Rev. C **104**, 014902 (2021).
[17] R. C. Hwa and L. Zhu, Phys. Rev. C **97**, 054908 (2018).
[18] L. Zhu, H. Zheng, K. Da, H. Gong, Z. Ye, G. Liu and R. C. Hwa, Phys. Rev. C **107**, 064907 (2023).
[19] L. Adamczyk *et al.* (STAR Collaboration), Phys. Rev. C 96 (2007) 044904.
[20] R. C. Hwa and L. Zhu, Phys. Rev. C **81**, 034904 (2010).
[21] J. Putschke (STAR Collaboration), J. Phys. G: Nucl. Part. Phys. **34**, S679 (2007).
[22] C. B. Chiu and R. C. Hwa, Phys. Rev. C **79**, 034901 (2009).
[23] R. C. Hwa and L. Zhu, Phys. Rev. C **84**, 064914 (2011).
[24] D. K. Srivastava, C. Gale and R. J. Fries, Phys. Rev. C **67** , 034903 (2003).
[25] L. Adamczyk *et al.* [STAR], Phys. Rev. C **93**, 014907 (2016).
[26] M. Abdallah *et al.* [STAR], Phys. Rev. C **105**, 064911 (2022).
[27] J. Adam *et al.* [ALICE], JHEP **09**, 164 (2016).
[28] S. Acharya *et al.* [ALICE], JHEP **09**, 006 (2018).